



Contents lists available at SciVerse ScienceDirect

Journal of Structural Biology

journal homepage: www.elsevier.com/locate/yjsbi

Laboratory cryo soft X-ray microscopy

H.M. Hertz^{a,*}, O. von Hofsten^a, M. Bertilson^a, U. Vogt^a, A. Holmberg^a, J. Reinspach^a, D. Martz^a, M. Selin^a, A.E. Christakou^a, J. Jerlström-Hultqvist^b, S. Svärd^b

^aBiomedical and X-Ray Physics, Dept. of Applied Physics, KTH Royal Inst. of Technology/Albanova, 10691 Stockholm, Sweden

^bDept. of Cell and Molec. Biol., Uppsala University, 75105 Uppsala, Sweden

ARTICLE INFO

Article history:
Available online xxxx

Keywords:
X-ray microscopy
Cryo fixation
Laboratory
Parasites

ABSTRACT

Lens-based water-window X-ray microscopy allows two- and three-dimensional (2D and 3D) imaging of intact unstained cells in their near-native state with unprecedented contrast and resolution. Cryofixation is essential to avoid radiation damage to the sample. Present cryo X-ray microscopes rely on synchrotron radiation sources, thereby limiting the accessibility for a wider community of biologists. In the present paper we demonstrate water-window cryo X-ray microscopy with a laboratory-source-based arrangement. The microscope relies on a $\lambda = 2.48$ -nm liquid-jet high-brightness laser-plasma source, normal-incidence multilayer condenser optics, 30-nm zone-plate optics, and a cryo sample chamber. We demonstrate 2D imaging of test patterns, and intact unstained yeast, protozoan parasites and mammalian cells. Overview 3D information is obtained by stereo imaging while complete 3D microscopy is provided by full tomographic reconstruction. The laboratory microscope image quality approaches that of the synchrotron microscopes, but with longer exposure times. The experimental image quality is analyzed from a numerical wave-propagation model of the imaging system and a path to reach synchrotron-like exposure times in laboratory microscopy is outlined.

© 2011 Elsevier Inc. All rights reserved.

1. Introduction

Determination of the structure of intact unstained cells with high spatial resolution is important for cell-biology. X-rays have the necessary absorption and scattering properties for two- and three-dimensional imaging of such thick (5–10 μm) objects. The two major X-ray imaging methods are lens-based soft X-ray microscopy (XRM) (Sakdinawat and Attwood, 2010) and lens-less hard X-ray coherent diffraction imaging (CDI) (Chapman and Nugent, 2010). Both require significant X-ray doses to provide the necessary signal-to-noise ratio for high-resolution imaging, making sample preparation and sample damage important issues. XRM (Uchida et al., 2009; Schneider et al., 2010) has shown 50–70 nm isotropic resolution in whole intact unstained cryo-fixed cells. The emerging hard X-ray CDI technique (Giewekemeyer et al., 2010; Jiang et al., 2010; Nelson et al., 2010) shows potential for similar detail but is still typically applied to freeze dried or fixed cells. Both methods can obtain higher resolution for smaller samples or smaller regions of interests within samples, albeit at the price of higher dose. Unfortunately, both methods presently rely on large-scale accelerator-based X-ray facilities, synchrotrons or free-electron lasers, thereby limiting the accessibility for a wider community of biologists. Present non-X-ray high-resolution

laboratory-scale methods, i.e., electron (Medalia et al., 2002) and super-resolution optical (Hell, 2009) microscopy, provide excellent resolution (tens of nanometers and below) but are essentially limited to thin objects due to electron scattering and long exposure times, respectively, and are thereby presently not applicable to intact cells. Thus, a laboratory-scale method that allows imaging of intact cells in their native or near-native hydrated state with a resolution of tens of nanometers has potential to fill an important void.

X-ray microscopy (XRM) in the water window ($\lambda = 2.3$ –4.4 nm; $E = 284$ –540 eV) has demonstrated high-resolution imaging of intact cells (Sakdinawat and Attwood, 2010; Kirz et al., 1995). Optically, the resolution in two-dimensional (2D) imaging is presently determined by the zone plate fabrication rather than the wavelength to typically 10–20 nm (Chao et al., 2005; Vila-Comamala et al., 2009). The contrast relies on the differential absorption between carbon (protein, lipids, etc.) and water, i.e., no staining is necessary. Detection of a statistically significant feature requires a certain signal-to-noise (cf. Rose criterion (Bushberg et al., 2002)) and, thus, a certain number of photons. Typically a water-window XRM image requires $\sim 10^6$ Gy for absorption imaging of 50 nm protein object in 10 μm of water under realistic assumptions (Kirz et al., 1995; Schneider, 1998). This can be lowered 0.5–1 order of magnitude by phase imaging. Hydrated biological samples show structural changes already at $\sim 10^4$ Gy (Schneider, 1998). Chemical fixation allows up $\sim 10^6$ Gy while cryo fixation has been shown to provide stable samples for $\sim 10^{10}$ Gy (Schneider

* Corresponding author. Fax: +46 8 55378466.

E-mail address: hertz@biox.kth.se (H.M. Hertz).

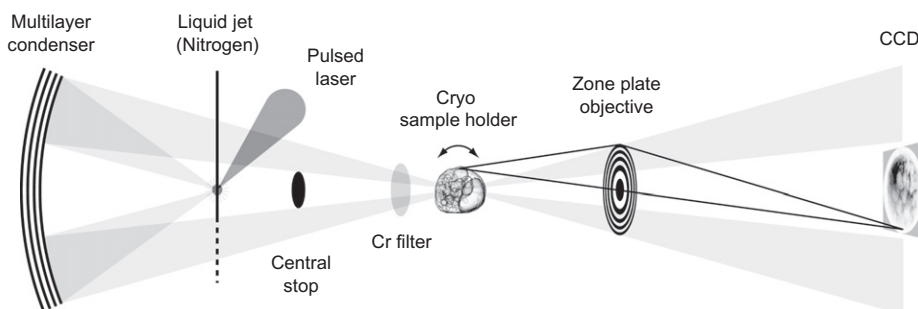


Fig. 1. Laboratory soft X-ray cryo microscopy arrangement. High-intensity laser pulses are focused onto a liquid-nitrogen jet, producing a line-emitting water-window soft-X-ray plasma. A normal-incidence multilayer mirror acts as combined monochromator and condenser, focusing the X-rays onto the sample. A zone plate, used in the first diffraction order, produces a high-resolution image on a CCD. Undiffracted X-rays are blocked by a central stop and scattered laser light is blocked by a filter. A cryo sample stage allows multi-angular image acquisition of biological samples, for subsequent reconstruction to 3D tomograms.

et al., 1995). This is important since the typical data acquisition for three-dimensional (3D) tomographic imaging at synchrotrons presently is at the 10^9 Gy level. Furthermore, it can be shown that the required dose scales as one over the feature size to the 4th power (Schneider, 1998). Thus, cryo sample preparation is essential for mitigating dose damage in X-ray microscopy, just as in electron microscopy.

Cryo fixation for 2D water-window X-ray microscopy was pioneered by Schneider (Schneider et al., 1995; Schneider, 1998). In the last few years, 3D imaging of cryogenically fixed cells has emerged (Weiss et al., 2000; Larabell and Le Gros, 2004) and is now delivering biologically relevant results (X-ray cryo tomography) (Uchida et al., 2009; Schneider et al., 2010). In addition to providing 3D images of intact hydrated cells in their near-native state, the method allows classification of different intra-cellular structures (e.g., lipid droplets, mitochondria, nuclei, vacuoles, etc.) due to quantitative determination of the local absorption coefficient (LAC) via Beer–Lambert’s law, in analogy to the macroscopic X-ray imaging of computed tomography. However, as stated in the Section 1, present cryo X-ray microscopes¹ rely on synchrotron radiation sources. Laboratory water-window X-ray microscopes based on zone plates and laser-plasma sources (Berghlund et al., 2000; Takman et al., 2007) have demonstrated test-object 2D imaging down to 25 nm resolution (von Hofsten et al., 2009), phase-contrast imaging (von Hofsten et al., 2008), and early 3D tomography on test objects (Bertilson et al., 2009) and recently on cryo-frozen necrotic cells (Bertilson, 2011b). Microscopes based on other laboratory sources or optics provide less detail (Benk et al., 2008; Hoshino and Aoki, 2008). For completeness, we note that table-top CDI systems (Sandberg et al., 2008) operate at wavelengths not applicable for biology.

In the present paper we describe our laboratory cryo soft X-ray microscope and analyze its capabilities. We demonstrate high-resolution 2D imaging of different types of intact and unstained cells (yeast, two types of protozoan parasites, and a mammalian cell), and show that the image quality (resolution and contrast) approaches that of synchrotron-based microscopes, albeit with longer exposure times. Finally, tomographic reconstruction provides 3D images that are quantitatively analyzed based on the local absorption coefficient (LAC).

2. Materials and methods

2.1. Overview

Fig. 1 describes the experimental arrangement. In brief, the microscope consists of a liquid-jet laser-plasma source, a normal-

incidence multilayer condenser, a tiltable cryo sample holder, a zone plate for the high-resolution imaging, and a CCD detector (Takman et al., 2007). The system operates at $\lambda = 2.48$ nm for highest water-window transmission in thick objects (Kirz et al., 1995; Takman et al., 2007). The 30 nm zone plate has a nominal Rayleigh resolution of 37 nm (full period) and provides sufficient depth-of-focus (DOF) to allow imaging of 50 nm features in ~ 5 μ m thick object. Biological samples were cultivated, harvested, and plunge cryo frozen according to standard procedure. 2D images are provided by single-angle exposures, stereo images from double-angle exposures and 3D tomograms are obtained from iterative tomographic reconstruction from multi-angular tilt series of 2D images.

2.2. Laboratory soft X-ray microscope

The $\lambda = 2.48$ nm water-window source was generated by focusing a $\lambda = 532$ nm, 150 mJ/pulse, 100 Hz, 3 ns Nd:YAG laser on a 20 μ m diameter liquid nitrogen jet (Jansson et al., 2005). The 20 \times 30 μ m FWHM plasma was imaged with 1.6 \times magnification onto the sample with a 58 mm diameter, $R = 300$ mm normal-incidence Cr/V multilayer mirror. The 0.6% reflectivity mirror selected the $\sim 10^{12}$ photons/(sr \times pulse), $\lambda/\Delta\lambda > 500$ hydrogen-like nitrogen K_{α} line at $\lambda = 2.48$ nm. A chromium filter separated the source and sample vacuum chambers and blocked scattered laser light, and a central stop produced hollow-cone illumination. A nickel zone plate with 30 nm outermost zone width, 825 zones, 1.2 mm focal length, and 99 μ m diameter formed the high-resolution image. The in-house fabricated zone plate (e.g., Reinspach et al., 2011) had a first-order diffraction efficiency of $\sim 9\%$ and a collection efficiency of $\sim 60\%$ due to the 1.5 \times overmatched condenser aperture. A magnification of 667 was used throughout the experiments, resulting in 20 nm object-plane pixels on the detector, a back-thinned, back-illuminated charge-coupled device (Princeton Instruments, 2048 \times 2048, 13 μ m). The hollow-cone illumination produced an area free of undiffracted (0th-order) intensity, defining the field-of-view. Typically, the system provides 500–1000 photons/pixel during 1 min of exposure.

2.3. Samples and sample preparation

The single-celled diplomonad parasite *Spironucleus salmonicida* (ATCC 50380), which causes systemic disease in farmed salmon populations, were grown in LYI *Giardia* medium (PRA-2155, ATCC) at 16 $^{\circ}$ C under microaerophilic conditions and imaged in the trophozoite state. The human intestinal parasite *Giardia intestinalis* WB clone C6 was cultivated in TYDK media (Keister, 1983) at 37 $^{\circ}$ C under microaerophilic conditions and imaged in the trophozoite stage. Human immune system B-cells (721.221/HLA-Cw6) were grown in cell culture medium at 37 $^{\circ}$ C and 5% CO_2 . All cells were harvested according to standard procedure, seeded to a

¹ National Center for X-ray Tomography, <http://www.ncxt.lbl.gov/>; BESSY II X-ray Microscope, http://www.bessy.de/bit/bit_station_list.php.

carbon-film-coated TEM grid, blotted to remove excess liquid, and finally plunge-frozen in liquid ethane. Protozoan cell viability (actively swimming cells, beating flagella) at the time of plunge freezing on the TEM grid was assessed by light microscopy. The dried yeast cells *Saccharomyces cerevisiae*, or common budding yeast, were rehydrated in water and sucrose solution before the plunge freezing. The samples were then transferred into the microscope and kept at cryogenic temperatures with a high-tilt transfer holder (Gatan) during the image acquisition. The sample stage was a modified transmission electron microscope goniometer stage (FEI), enabling 180-degree rotation of commercially available TEM sample holders, while the used sample-objective geometry limited the acquisition angles to $\pm 50^\circ$ for the tomography. Liquid nitrogen-cooled copper shields surrounded the sample environment to ensure low water residuals. An optical microscope was positioned above the sample for visual alignment and inspection. The absorbed dose by a sample is typically 1 MGy for a 2D image and 10–50 MGy for a full tilt series for tomography.

2.4. Image acquisition and processing

The 2D images were typically recorded with multiple exposures for a total of 5–10 min. They are corrected for non-uniform illumination. 3D tomograms were obtained from a multi-angular tilt-series of 2D images, each typically with 30 s exposure time. The images were normalized to compensate for illumination fluctuations, aligned (land-marked), and the projected densities, $P_\theta = -\log(I_\theta/I_0)$, were calculated from image intensities I_θ and an estimated incident intensity I_0 . The 3D local absorption coefficient (LAC) was finally reconstructed from these (slightly denoised) projected densities using a simultaneous iterative reconstruction technique (SIRT) (Bertelson et al., 2011b). The missing wedge of the present arrangement caused underestimation of LAC outside the cells. All reconstructions were performed with 40 nm cubic voxels and 60 iterations. Alignments and reconstructions were performed with the TomoJ (Messaoudil et al., 2007) plugin for ImageJ (Rasband, 1997). AMIRA[®] was used for semi-manual segmentation, surface rendering, and visualization.

3. Results

3.1. Two-dimensional imaging

Fig. 2 shows a Siemens-star test pattern, imaged when attached to the cryo sample holder. The 17 μm diam gold pattern has a center line width of 25 nm (50 nm full period). As expected, the zone-plate optics of the microscope resolves this pattern but one can also observe slightly lower effective resolution in one direction, probably due to residual vibrations in the system.

Fig. 3 shows examples of laboratory soft X-ray microscopy of intact cells, prepared with cryo fixation in their natural environment and without staining or slicing. Fig. 3a shows yeast cells later used for tomographic reconstruction. Fig. 3b depicts a small dense cell, the protozoan parasite *S. salmonicida*. The flagella as well as sub-cellular structures in the carbon-rich cell body are clearly visible and the thin ice layer does not affect the image quality. Vesicular structures, not seen in light microscopy, are clearly visible, as are the flagellar canals. Fig. 3c shows another protozoan parasite, *G. intestinalis*. The parasite is in the trophozoite form and in the cytokinesis stage of the cell cycle, seen by the cell size, number of flagella and an intact adhesive disc and nuclei. Fig. 3d shows a larger and less dense sample, a human immune system B-cell. The nuclei and a few nucleoli are clearly visible. The image shows enhanced contrast and detail compared to optical microscopy, especially for the dense, round sub-micron structures which most likely are

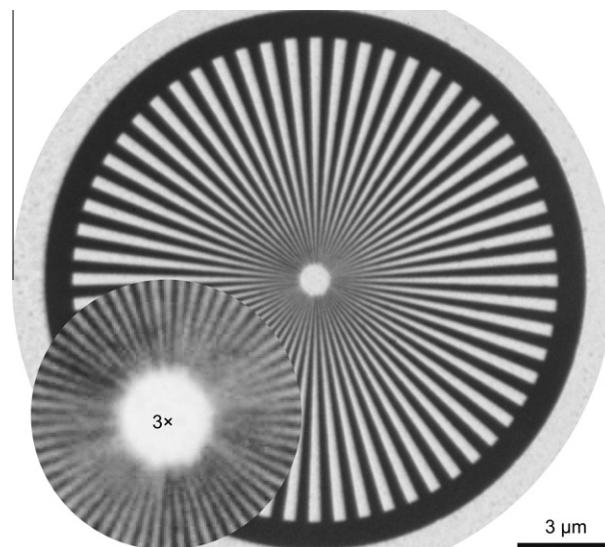


Fig. 2. Image of gold test pattern. The line width in the center is 25 nm.

protein-dense granules. The four examples demonstrate that laboratory cryo X-ray microscopy can provide 2D images with synchrotron-like quality of a wide range of intact thick biological samples. While yeast and *Giardia* parasites have been studied previously at synchrotron-based X-ray microscopes (Uchida et al., 2009; Kozek et al., 2003) the human B cell and the *Spironucleus* have not been imaged previously with X-ray microscopy. The detail and contrast achievable appear to make comparisons with other 2D microscopy techniques potentially fruitful.

3.2. Stereo imaging

Stereo imaging provides an overview of the depth structure by comparing the relative positions of specific features when viewed from two angles. Fig. 4 shows a stereo image pair of *Spironucleus* parasites. The vertical tilt between the images is 16° . Naturally, the method does not provide the same 3D spatial detail as with tomography (cf. Section 3.3). Often, however, such overview depth information is sufficient for a first quick assessment. The mode of imaging is especially important for the present laboratory microscope arrangement where the acquisition of several tens of projections for tomography may be excessively time-consuming. Gleber et al. (2009) has shown that the basic spatial distribution and 3D proximity relation in the range of 50–500 nm can be obtained with a reasonable computational effort for soil samples.

3.3. Three-dimensional tomographic imaging

The tomographic 3D cryo microscopy is based on reconstruction using 2D images as projections. Thus, high-quality 2D microscopy and appropriate sample preparation is a prerequisite for high-quality 3D tomograms. Fig. 5 shows 3D tomograms of yeast cells reconstructed from tilt series of 2D images from the laboratory microscope. Here 207 projections, each with 30 s exposure time, over $\pm 51.5^\circ$ was used. Fig. 5a shows a slice through the reconstruction. The grayscale corresponds to the local absorption coefficient (LAC). The yeast cells are small and are therefore imaged accurately within the $\sim 5\text{-}\mu\text{m}$ DOF. The smallest observable features are close to ~ 100 nm and limited by noise. In Fig. 5b the intracellular structures have been segmented according to the LAC, differentiating, e.g., nucleus and vacuoles, and visualized by surface rendering techniques. Note the thick wall of two of the cells (e.g., #1), typical of spores, and a possible slight swelling of the other three, due to

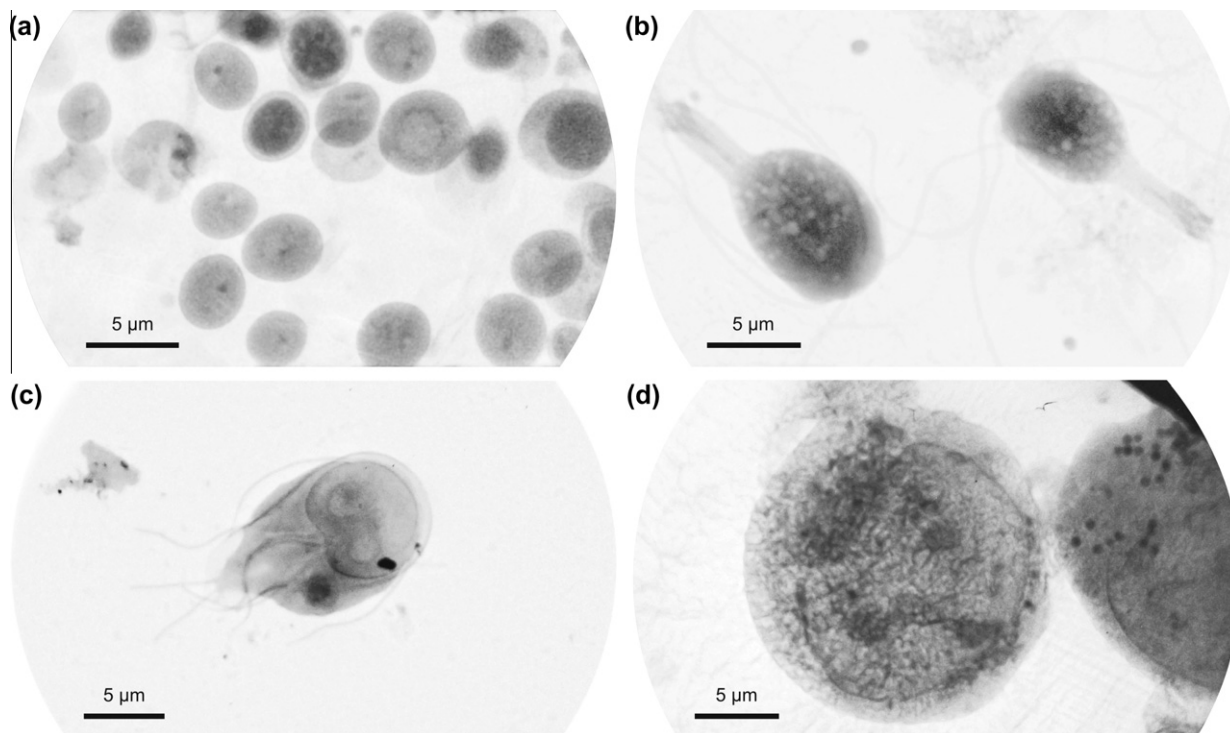


Fig. 3. Laboratory X-ray microscopy of cryo-fixed cells. 2D images of intact non-stained cells. (a) Budding yeast cells. (b) *Spiroplasma salmonicida* parasites. (c) *Giardia intestinalis* parasites. (d) A human immune system B-cell. All show considerable intra-cellular structures and detail with natural contrast.

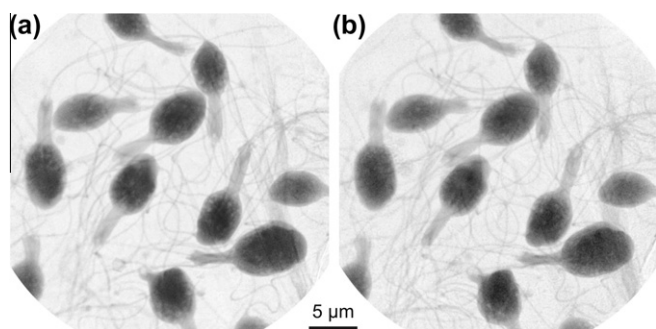


Fig. 4. Stereo image pair of *Spiroplasma* parasites. The angle between the views is 16° around the vertical axis.

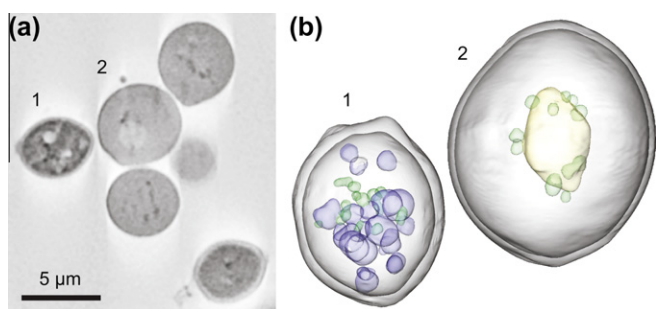


Fig. 5. 3D imaging with laboratory X-ray cryo microscopy. (a) Orthoslice through a tomogram of a yeast cell sample. It was reconstructed from 207×30 s exposures, covering $\pm 51.5^\circ$. A higher local absorption coefficient (LAC) corresponds to darker gray. (b) Surface rendering of segmented cellular features for cells #1 and #2. Color coding is based on the LAC and indicates nucleus (yellow), vacuoles (blue), and other organelles with higher LAC (green).

the preparation method. 3D animated section scans and surface renderings are provided as Video Files. In Bertilson et al. (2011b) the method is proof-of-principle demonstrated for larger diameter object (a $13 \mu\text{m}$ necrotic human kidney cell), probably with decreased accuracy since part of the object is out of focus.

4. Discussion

4.1. 2D image quality

It is well known that image quality in 2D X-ray microscopy relies on zone-plate resolution, signal-to-noise ratio, and sample preparation. The test pattern image (Fig. 2) supports the expected nominal full-period Rayleigh resolution of 37 nm for the 30 nm zone plate. The transmitted photon flux is maximized for improved Poisson signal-to-noise ratio by operating at $\lambda = 2.48 \text{ nm}$ for highest water-window transmission in thick objects (Kirz et al., 1995; Takman et al., 2007). The biological samples were cultivated, harvested, and plunge cryo frozen according to standard procedure and show very limited ice crystal formation and no radiation damage. Here image features down to the 100-nm range are visible and the flagellas are 200 nm wide, similar to what is observed in electron microscopy (Jorgensen and Sterud, 2006; Benchimol et al., 2004).

However, a more detailed analysis of image quality (resolution and contrast) must include also effects of DOF, partial coherence and stray light. Bertilson et al. (2011a) provides a numerical model for such an analysis. From this we can conclude that the present arrangement, with a slightly overmatched condenser numerical aperture (NA) (coherence parameter $m = 1.5$, where $m = NA_{\text{condenser}}/NA_{\text{zone plate}}$) provide very high resolution over a limited DOF and with a somewhat low contrast. By reducing the condenser NA and making the illumination partially coherent ($m < 1$) the DOF and the contrast can be increased but at the price of increasing interference-induced artifacts in the image. This has

been favorably used in, e.g., Schneider et al. (2010) to improve detectability of, e.g., intracellular membranes. Finally, the stray light needs to be limited since it reduces contrast. It can be shown that it increases with source size and decreases with focal length. The present zone plate/source size combination was chosen for its combination of low stray light and high collection efficiency.

4.2. 3D image quality

The most important difference between classical computed tomography (CT) and the present zone-plate X-ray cryo-microscope-based tomography system is that CT ideally relies on geometrical projections while the tomographic reconstruction here is based on images. Thus, effects of DOF, partial coherence, and stray light on the 2D images will influence the 3D reconstructions. Consequently, the accuracy of the reconstructed LAC depends on the optical system as well as the feature size and sample radius. For example, a low NA zone plate provides the more accurate reconstruction for most features in a large object, due to its longer DOF, while a high NA zone plate gives a better modulation and resolution in the center. The limited DOF of such a zone plate leads to a decrease of the modulation with the radius. Thus, the correct classification of intracellular structures (e.g., Uchida et al., 2009; Bertilson et al., 2011b) cannot be based on the calculated LAC alone but must include also other experimental parameters as well as cell biological knowledge.

4.3. Exposure time

The major present disadvantage of the laboratory cryo X-ray microscope is the long exposure times. Not only does it make routine imaging of large sample numbers impractical but image quality also deteriorates due to (inevitable) thermal drifts and/or low signal-to-noise ratio. These problems are especially pronounced in the tomographic data acquisition. Compared to the typical few-to-several-second single-image exposure time at synchrotron microscopes, the present laboratory microscope often requires 20–50× longer time.

We presently attempt to shorten exposure times to the 10-s regime. The major improvement is a new high-average-power laser for a higher-brightness laser-plasma source. This 2 kHz, 100 mJ/pulse, 600 ps pulsed diode-pumped slab-amplified Nd:YAG laser increases the average X-ray power both by its higher average power (>200 W cf. to 15 W in this paper) and the higher pulse intensity (100 mJ at 0.6 ns cf. to 130 mJ at 3 ns), which will provide a more appropriate plasma temperature for our emission energies. The high repetition rate and the high average power puts severe demands on the target system, which must deliver fresh target material with high spatial accuracy (<5 μm) to each new shot. Here we benefit from the high-speed (50 m/s) of liquid-nitrogen-jet system and earlier studies indicating that the liquid jets are stable also at kHz laser repetition rates (Korn et al., 2002). We anticipate, however, that significant efforts on the thermal management, both for minimum laser beam distortion and for the target system, will be necessary. We expect the new laser-plasma source system to ultimately reduce the present exposure times with a factor 10 or more, i.e., bringing laboratory X-ray microscopes close to synchrotron-like exposure times.

The other major source for improvement is the optics. We believe it is possible to increase the reflectivity of the multilayer condenser by a factor 2–3, and to increase the efficiency of the zone plate by a factor 2, by multi-material zone plates (Reinspach et al., 2011). Together, these improvements would lead to sub-ten second exposure times for laboratory cryo X-ray microscopy of intact cells. More speculative is the use of phase contrast for reduced dose and, thus, reduced exposure time, since the field of view may

be too limited and background scattering may reduce the expected gain (von Hofsten et al., 2009).

5. Conclusion

We have shown that laboratory cryo soft X-ray microscopy allows high-resolution imaging of unstained intact cells with a quality approaching that of synchrotron-based microscopes. 2D imaging is demonstrated to provide natural contrast and high resolution on a wide range of cells while 3D tomographic reconstruction allows quantitative classification of structure via local absorption coefficient (LAC). Modeling together with our experiments show that the proper choice of system parameters (such as zone-plate optics, condenser and source) depends on the object (e.g., size, composition, structure) and the imaging goals. Thus, the microscope optics-and-source parameters should be optimized for each object-and imaging problem in order to reach highest resolution and contrast. From the model we estimate that a resolution approaching 30 nm (half-period) over full 5-μm diameter objects such as small cells should be achievable in tomography while 2D imaging is limited by the X-ray optical system. Such high-resolution quantitative 2D and 3D imaging of intact cells in their hydrated near-native state is of significant importance for studies of the function and structure of biological material on the nanoscale. The laboratory-scale of the instrument increase accessibility and, thus, potential scientific impact. The major limitation of the present system is the long exposure times, which we hope to decrease in the near future. This would allow high-resolution 2D and 3D cryo biological imaging of intact cells in the local laboratory with synchrotron-like properties, both as regards exposure time and image quality.

Acknowledgments

This work was supported by the Swedish Research Council, the Swedish Foundation for Strategic Research, and the Wallenberg Foundation. We thank Magnus Lindblom for early zone plates and Hjalmar Brismar for discussions.

Appendix A. Supplementary data

Supplementary data associated with this article can be found, in the online version, at doi:10.1016/j.jsb.2011.11.015.

References

- Benchimol, M., Piva, B., Campanati, L., de Souza, W., 2004. Visualization of the funis of *Giardia lamblia* by high-resolution field emission scanning electron microscopy—new insights. *J. Struct. Biol.* 147, 102–115.
- Benk, M., Bergmann, K., Schäfer, D., Wilhein, T., 2008. Compact soft X-ray microscope using a gas-discharge light source. *Opt. Lett.* 33, 2359–2361.
- Berglund, M., Rymell, L., Peuker, M., Wilhein, T., Hertz, H.M., 2000. Compact water-window transmission X-ray microscopy. *J. Microsc.* 197, 268–273.
- Bertilson, M., von Hofsten, O., Vogt, U., Holmberg, A., Hertz, H.M., 2009. High-resolution computed tomography with a compact soft X-ray microscope. *Opt. Express* 17, 11057–11065.
- Bertilson, M., von Hofsten, O., Hertz, H.M., Vogt, U., 2011a. Numerical model for tomographic image formation in transmission X-ray microscopy. *Opt. Express* 19, 11578.
- Bertilson, M., von Hofsten, O., Vogt, U., Holmberg, A., Christakou, A., et al., 2011b. Laboratory soft x-ray microscope for cryo tomography of biological specimens. *Opt. Lett.* 36, 2728.
- Bushberg, J.T., Seibert, J.A., Leidholdt, E.M., Boone, J.M., 2002. *The Essential Physics of Medical Imaging*. Lippincott Williams & Wilkins, Philadelphia, PA.
- Chao, W., Harteneck, B.D., Liddle, J.A., Anderson, E.H., Attwood, D.T., 2005. Soft X-ray microscope at a spatial resolution better than 15 nm. *Nature* 435, 1210–1213.
- Chapman, H.N., Nugent, K.A., 2010. Coherent lens-less X-ray imaging. *Nat. Phot.* 4, 833–839.
- Coluccio, A., Neiman, A.M., 2004. Interspore bridges: a new feature of *Saccharomyces cerevisiae* spoer wall. *Microbiology* 150, 3189–3196.
- Giewekemeyer, K., Thibault, P., Kalbfleisch, S., Beerlink, A., Kewish, C.M., et al., 2010. Quantitative biological imaging by Ptychographic x-ray diffraction microscopy. *Proc Natl Acad Sci USA* 107, 529–534.

- Gleber, S.-C., Thieme, J., Chao, W., Fischer, P., 2009. Stereo soft x-ray microscopy and elemental mapping of hematite and clay suspensions. *J. Micr.* 235, 199–208.
- Hell, S.W., 2009. Microscopy at its focal switch. *Nat. Methods* 6, 24–32.
- Hoshino, M., Aoki, S., 2008. Laboratory-Scale Soft X-ray Imaging Microtomography Using Wolter Mirror Optics. *Appl. Phys. Express* 1, 067005-1-3.
- Jansson, P.A.C., Vogt, U., Hertz, H.M. 2005. Liquid-nitrogen-jet laser-plasma source for compact soft x-ray microscopy. *Rev. Sci. Instrum.* 76, 43503 1-5.
- Jiang, H., Song, C., Chen, C.-C., Xu, R., Raines, K.S., et al., 2010. Quantitative 3D imaging of whole, unstained cells by using X-ray diffraction microscopy. *Proc. Natl. Acad. Sci. USA* 107, 11234–11239.
- Jorgensen, A., Sterud, E., 2006. The marine pathogenic genotype of *Spironucleus barkhanus* from farmed salmonids redescribed as *Spironucleus salmonicida* n. sp. *J. Eukaryot. Microbiol.* 53, 531–541.
- Keister, D.B., 1983. Axenic culture of *Giardia lamblia* in TYI-S-33 medium supplemented by bile. *Trans. R. Soc. Trop. Med. Hyg.* 77, 487–488.
- Kirz, J., Jacobsen, C., Howells, M., 1995. Soft-X-ray microscopes and their biological applications. *Quart. Rev. Biophys.* 28, 33–130.
- Korn, G., Thoss, A., Stiel, H., Vogt, U., Richardson, M., Elsaesser, T., Faubel, M., 2002. Ultrashort 1-kHz laser plasma hard x-ray source. *Opt. Lett.* 27, 866–868.
- Kozek, W.J., Nair, A., Denbeaux, G., Larabell, C., Brown, J., et al., 2003. Soft X-ray microscopy; a new technology for examination of parasitic specimen. *Microsc. Microanal.* 9, 1452.
- Larabell, C.A., Le Gros, M.A., 2004. X-ray tomography generates 3-D reconstructions of the yeast, *Saccharomyces cerevisiae*, at 60-nm resolution. *Mol. Biol. Cell* 15, 957–962.
- Medalia, O., Weber, I., Frangakis, A.S., Nicastro, D., Gerisch, G., et al., 2002. Macromolecular architecture in eukaryotic cells visualized by cryoelectron tomography. *Science* 298, 1209–1213.
- Messaoudil, C., Boudier, T., Sorzano, C., Marco, S., 2007. Tomoj: tomography software for three-dimensional reconstruction in transmission electron microscopy. *BMC Bioinf.* 8288, 1–9.
- Nelson, J., Huang, X., Steinbrener, J., Shapiro, D., Kirz, J., et al., 2010. High-resolution X-ray diffraction microscopy of specifically labeled yeast cells. *Proc. Natl. Acad. Sci. USA* 107, 7235–7239.
- Rasband, W.S., 1997–2009. ImageJ, US National Institutes of Health, <<http://info.nih.gov/ij/>>.
- Reinspach, J., Lindblom, M., Bertilson, M., von Hofsten, O., Hertz, H.M., et al., 2011. 13-nm high efficiency nickel-germanium soft X-ray zone plates. *J. Vac. Sci. Tech. B* 29, 011012 1–4.
- Sakdinawat, A., Attwood, D., 2010. Nanoscale X-ray imaging. *Nat. Photonics* 4, 840–848.
- Sandberg, R.L., Song, C., Wachulak, P.W., Raymondson, D.A., Paul, A., et al., 2008. High numerical aperture tabletop soft X-ray diffraction microscopy with 70 nm resolution. *Proc. Natl. Acad. Sci. USA* 105, 24–27.
- Schneider, G., 1998. Cryo X-ray microscopy with high spatial resolution in amplitude and phase contrast. *Ultramicroscopy* 75, 85–104.
- Schneider, G., Niemann, B., Guttman, P., Rudolph, D., Schmahl, G., 1995. Cryo X-ray microscopy. *Synchrotron Radiat. News* 8, 19–28.
- Schneider, G., Guttman, P., Heim, S., Rehbein, S., Mueller, et al., 2010. Three-dimensional cellular ultrastructure resolved by X-ray microscopy. *Nat. Methods* 7, 985–987.
- Takman, P.A.C., Stollberg, H., Johansson, G.A., Holmberg, A., Lindblom, M., et al., 2007. High-resolution compact X-ray microscopy. *J. Microsc.* 226, 175–181.
- Uchida, M., McDermott, G., Wetzler, M., Le Gros, M.A., Myllys, et al., 2009. Soft X-ray tomography of phenotypic switching and the cellular response to antifungal peptoids in *Candida albicans*. *Proc. Natl. Acad. Sci. USA* 106, 19375–19380.
- Vila-Comamala, J., Jefimovs, K., Raabe, J., Pilvi, T., Fink, R.H., et al., 2009. Advanced thin film technology for ultrahigh resolution X-ray microscopy. *Ultramicroscopy* 109, 1360–1364.
- von Hofsten, O., Bertilson, M., Holmberg, A., Vogt, U., 2008. Compact Zernike phase contrast X-ray microscopy using a single-element optic. *Opt. Lett.* 33, 932–934.
- von Hofsten, O., Bertilson, M., Reinspach, J., Holmberg, A., Hertz, H.M., et al., 2009. Sub-25-nm laboratory X-ray microscopy using a compound Fresnel zone plate. *Opt. Lett.* 34, 2631–2633.
- Weiss, D., Schneider, G., Niemann, B., Guttman, P., Rudolph, D., et al., 2000. Computed tomography of cryogenic biological specimens based on X-ray microscopic images. *Ultramicroscopy* 84, 185–197.